Volume 5 | Number 36 | 28 September 2017 | Pages 18899–19502

Journal of Materials Chemistry A

Materials for energy and sustainability

rsc.li/materials-a

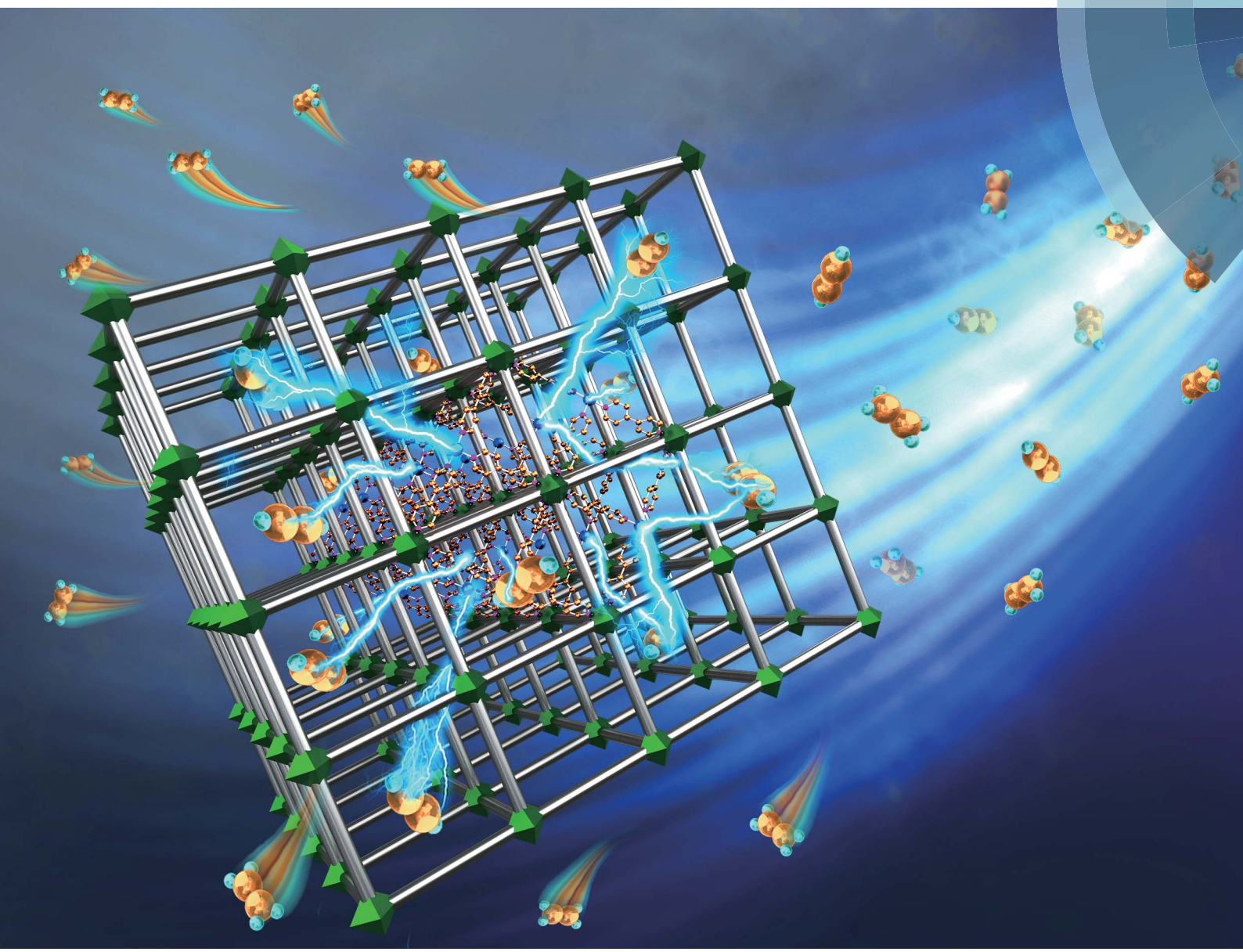

ISSN 2050-7488

ROYAL SOCIETY OF CHEMISTRY

PAPER

Jinping Li, Wei Zhou, Banglin Chen *et al.*

Efficient separation of ethylene from acetylene/ethylene mixtures by a flexible-robust metal–organic framework

Journal of Materials Chemistry A

PAPER

View Article Online
View Journal | View Issue

Cite this: J. Mater. Chem. A, 2017, 5, 18984

Efficient separation of ethylene from acetylene/ethylene mixtures by a flexible-robust metal–organic framework†

Libo Li,[abe] Rui-Biao Lin,[b] Rajamani Krishna,[c] Xiaoqing Wang,[ae] Bin Li,[b] Hui Wu,[d] Jinping Li,*[ae] Wei Zhou*[d] and Banglin Chen*[b]

Received 28th June 2017
Accepted 24th July 2017

DOI: 10.1039/c7ta05598f

rsc.li/materials-a

During the production of polymer-grade ethylene, trace amounts of acetylene (about 1%) in the ethylene feed need to be reduced to 40 parts per million (ppm). We herein report a metal–organic framework (MOF) of flexible-robust nature for the efficient removal of acetylene from acetylene/ethylene mixture to meet such a challenging separation need. Neutron powder diffraction studies reveal that its specific binding sites and unique pore structure collectively enable this MOF (ELM-12) to efficiently and selectively adsorb acetylene over ethylene under ambient conditions, making it feasible for this challenging separation. The purity of obtained ethylene is over 99.999%, as demonstrated by experimental breakthrough curves of 1/99 acetylene/ethylene mixture.

Introduction

Nowadays, oil and natural gas resources are supplying human needs worldwide. Large quantities of chemicals in the petrochemical industry are produced and purified into purer forms, and these separation processes account for 10–15% of the world's energy consumption.[1] Ethylene (C_2H_4), one of the most widely used organic chemicals in the world, is produced by steam cracking in the petroleum refining process. In the production of polymer-grade C_2H_4, the removal of trace acetylene (C_2H_2) (about 1%) from C_2H_4 gas must meet the requirement of ≤40 parts per million (ppm) C_2H_2 for the downstream polymerization reaction.[2,3] Traditional methods, such as cryogenic distillation and partial hydrogenation of C_2H_2, are energy intensive, so there is an urgent need to develop efficient adsorbents for C_2H_2 capture from C_2H_4.

In recent years, metal–organic frameworks (MOFs) with porous structures and designable frameworks have received considerable attention, as they offer great opportunities for revolutionizing some industrial applications, especially in the storage, separation and purification of gases.[4–12] Indeed, based on their sieving and preferential binding effects, a number of microporous MOFs have shown great promise for effective C_2H_2/C_2H_4 separation *via* pore tuning and functionalization. In 2011, Xiang *et al.* reported the first example of microporous MOFs for the efficient separation of C_2H_2/C_2H_4 mixtures.[13] Based on the sieving effect, M'MOF-3a enabled the full entrance of the smaller-sized C_2H_2 and basically blocked C_2H_4 molecules, exhibiting high C_2H_2/C_2H_4 selectivity, but the relatively low uptake of C_2H_2 restricted its separation capacity. Later, Hu *et al.* reported a microporous MOF UTSA-100 which can exhibit highly efficient removal of acetylene from C_2H_2/C_2H_4 (1/99) mixtures.[3] UTSA-100 has the special zigzag narrow channels (window opening 3.3 Å) and $-NH_2$ functionalized pore channels, which collaboratively enabled high C_2H_2/C_2H_4 selectivity and high C_2H_2 uptake capacity at low pressure, based on both sieving and preferential binding effects.[3] Very recently, the report of SIFSIX materials represented great progress in C_2H_2/C_2H_4 separation, where the preferential binding and orderly assembly of C_2H_2 molecules through cooperative host–guest and/or guest–guest interactions allow unprecedented performance in the separation of trace amounts of C_2H_2 from C_2H_4 gas mixtures.[2] Hence, strong binding sites and suitable pore size in robust MOFs are considered to be useful for C_2H_2 separation. Note, however, that higher adsorption affinity (isosteric heat of adsorption) will lead to greater energy costs during the regeneration process.[14,15] Therefore, generally, ideal porous materials for gas separation should exhibit high

[a]College of Chemistry and Chemical Engineering, Taiyuan University of Technology, Taiyuan 030024, Shanxi, P. R. China. E-mail: jpli211@hotmail.com
[b]Department of Chemistry, University of Texas at San Antonio, One UTSA Circle, San Antonio, TX 78249-0698, USA. E-mail: Banglin.Chen@utsa.edu
[c]Van't Hoff Institute for Molecular Sciences, University of Amsterdam, Science Park 904, 1098 XH Amsterdam, The Netherlands
[d]NIST Center for Neutron Research, National Institute of Standards and Technology, Gaithersburg, MD 20899-6102, USA. E-mail: wzhou@nist.gov
[e]Shanxi Key Laboratory of Gas Energy Efficient and Clean Utilization, Taiyuan 030024, Shanxi, P. R. China

† Electronic supplementary information (ESI) available: Powder XRD patterns, adsorption selectivities of C_2H_2/C_2H_4 (50/50) predicted by IAST at 298 K, regenerability and structural stability data of ELM-12. CCDC 1545783. For ESI and crystallographic data in CIF or other electronic format see DOI: 10.1039/c7ta05598f

adsorption selectivity and large adsorption capacity for the target gas molecules,[16–23] as well as relatively low adsorption heat for easy regeneration.

Herein, we report a microporous MOF $[Cu(bpy)_2(OTf)_2]$[24–26] (ELM-12, bpy = 4,4′-bipyridine, OTf^- = trifluoromethanesulfonate) with a flexible-robust structure for the efficient removal of trace C_2H_2 from C_2H_4 mixtures. This type of flexible-robust MOF is different from traditional flexible and robust MOFs in that their guest-free phases or intermediate phases possess robust pore structures. At relative low pressure, such flexible-robust MOFs will exhibit adsorbate-dependent gas sorption isotherms and thus can be theoretically applied to gas separation, which has basically been overlooked. ELM-12 exhibits high C_2H_2/C_2H_4 selectivity and low C_2H_2 adsorption heat, which is very good for practical gas separation applications. The special binding affinity and suitable pore confinement for C_2H_2 account for its high C_2H_2/C_2H_4 selectivity, as clearly evidenced by neutron powder diffraction studies. Its separation potential has been further established by IAST calculations and transient separation experiments. The trace amounts of C_2H_2 can be readily removed from a C_2H_2/C_2H_4 (1/99) mixture to produce high-purity C_2H_4 (over 99.999%) under ambient conditions.

Experimental section

Materials

$[Cu(bpy)_2(OTf)_2]$ (ELM-12): the synthetic method described by Kondo *et al.* was improved as follows:[25] A solution of bpy (10.0 mmol L^{-1}, 10.0 mL) in ethanol was carefully layered onto an aqueous solution of $Cu(OTf)_2$ (5.0 mmol L^{-1}, 10.0 mL) in a watch glass with no stirring. Then, the mixture was placed in a 298 K incubator for 7 days to give sheet crystals as $[Cu(bpy)_2(OTf)_2]\cdot 2EtOH\cdot H_2O$. Then, the crystals were collected and activated under 10^{-6} bar at 393 K until no further weight loss was observed, to give $[Cu(bpy)_2(OTf)_2]$ as a guest-free material.

Characterization

The crystallinities and phase purities of the samples were measured by powder X-ray diffraction (PXRD) with a Rigaku Mini Flex II X-ray diffractometer employing Cu K_α radiation operated at 30 kV and 15 mA, scanning over the range of 5–40° (2θ) at a rate of 1° min^{-1} (Fig. S1†).

Single-component adsorption measurements

Ultrahigh-purity-grade C_2H_2 and C_2H_4 were used for all measurements. Their adsorption isotherms were collected with an Intelligent gravimetric analyser (IGA 001, Hiden, UK). Samples were activated overnight under reduced pressure at 393 K or until no further weight loss was observed.

Neutron diffraction experiment

Powder neutron diffraction data were collected using the BT-1 neutron powder diffractometer at the National Institute of Standards and Technology (NIST) Center for Neutron Research. To probe the C_2H_2 adsorption locations, fully activated ELM-12 sample was loaded in a vanadium can, and a pre-determined pressure (1 bar) of C_2D_2 was loaded into the sample at room temperature. Diffraction data were then collected on the C_2D_2-loaded MOF sample, and Rietveld structural refinement was performed on the data. Both the ELM-12 building block and C_2D_2 molecules were treated as rigid bodies in Rietveld refinement (to limit the number of variables), with the molecule orientation and centre of mass freely refined. Refinement on lattice parameters, atomic coordinates, thermal factors, gas molecule occupancies, background, and profiles all converge with satisfactory *R*-factors. CCDC 1545783† contains the supplementary crystallographic data of C_2D_2-loaded ELM-12. This data can be obtained free of charge from the Cambridge Crystallographic Data Centre *via* http://www.ccdc.cam.ac.uk/data_request/cif.

Breakthrough separation experiments and procedures

The experimental setup consisted of two fixed-bed stainless steel reactors (Fig. S2†), each with inner dimensions of $\phi 9 \times 150$ mm, connected in parallel.[26,27] The horizontal reactors were placed in a temperature-controlled environment maintained at 298 K. The gas flow and pressure were set and controlled at the outlet and inlet by a pressure controller valve and a mass flow meter, and a gas chromatograph continuously monitored the effluent gas from the adsorption bed. For practical considerations, powder samples of ELM-12 were pelletized into particles of a certain size (220–320 μm), and the column was loaded with particles of ELM-12 (4.1380 g). To ensure the homogeneous nature of the synthesized materials, samples from all batches were tested by powder X-ray diffraction.

Result and discussion

Adsorption performance of C_2H_2 and C_2H_4 on ELM-12

We examined the C_2H_2 and C_2H_4 gas adsorption isotherms of ELM-12 at ambient temperatures of 273 and 298 K under 1 bar in order to figure out its potential for C_2H_2/C_2H_4 separation. As shown in Fig. 1, ELM-12 rapidly adsorbs C_2H_2 at low pressure ($\leq$0.1 bar), and its C_2H_2 uptake reaches 30.1 $cm^3\ g^{-1}$ (298 K) and 38.3 $cm^3\ g^{-1}$ (273 K) at 0.1 bar. With increasing pressure, stepwise adsorption appears at 0.25 bar for 298 K and 0.11 bar for 273 K (Fig. 1a and c), which indicates a slight structural transformation during C_2H_2 adsorption because of the certain flexibility of this MOF.[28–34] At 1 bar and 298 K, the uptake of ELM-12 for C_2H_2 is up to 57.3 $cm^3\ g^{-1}$. Surprisingly, ELM-12 adsorbs much smaller amounts of C_2H_4 (5.9 $cm^3\ g^{-1}$ at 0.1 bar and 22.5 $cm^3\ g^{-1}$ at 1 bar) at 298 K, which implies weaker interactions between the C_2H_4 molecule and ELM-12. The obvious difference between C_2H_2 and C_2H_4 adsorption indicates that ELM-12 is very promising for the removal of C_2H_2 from C_2H_4 mixtures.

To predict the C_2H_2/C_2H_4 separation performance of ELM-12 and compare it with other materials, ideal adsorbed solution theory (IAST) calculations were conducted on the C_2H_2/C_2H_4 (1/99 and 50/50) mixtures (Fig. 1b and S3†). Fig. 1d shows the

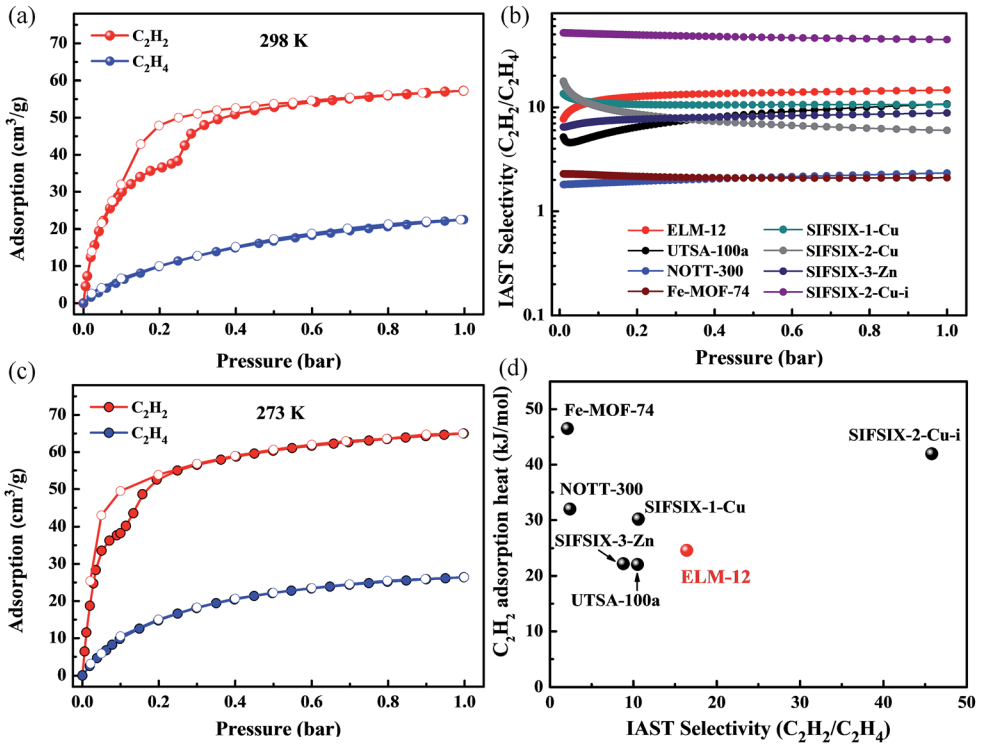

Fig. 1 C_2H_2 (red) and C_2H_4 (blue) sorption isotherms for ELM-12 at (a) 298 K and (c) 273 K. (b) Comparison of the IAST selectivities in C_2H_2/C_2H_4 (1/99) mixtures and (d) adsorption heat of ELM-12 *versus* those of previously reported best-performing materials for C_2H_2/C_2H_4 separation.

comparison of IAST selectivity and adsorption enthalpy calculated for ELM-12 and other reported materials. The C_2H_2/C_2H_4 adsorption selectivity of ELM-12 was calculated to be 14.8 at 1 bar, which is higher than those of previously reported MOFs except SIFSIX-2-Cu-i.

IAST separation selectivity values of the C_2H_2/C_2H_4 (1/99) mixture at 1 bar decrease in the order of SIFSIX-2-Cu-i > ELM-12 > SIFSIX-1-Cu > UTSA-100a > SIFSIX-3-Zn > SIFSIX-2-Cu > NOTT-300 > Fe-MOF-74. Other than gas separation selectivity, the energy required to regenerate the sorbent during the regeneration process is also very important for practical applications. Interestingly, compared to other materials, ELM-12 exhibits a quite modest adsorption enthalpy (Q_{st}) of 25.4 kJ mol^{-1} at zero-coverage (Fig. 1d), which is significantly lower than those of SIFSIX-2-Cu-i (42.0 kJ mol^{-1}) and Fe-MOF-74 (46.5 kJ mol^{-1}). This indicates that the interactions between C_2H_2 molecules and $CF_3SO_3^-$ anions in ELM-12 are comparatively weak and not as strong as those between C_2H_2 molecules with SiF_6^{2-} in SIFSIX-2-Cu-i or open Fe(II) sites in Fe-MOF-74. Overall, ELM-12 stands out as one of the best materials for the separation of C_2H_2/C_2H_4, given the fact that it exhibits moderately high C_2H_2 uptake and selectivity, but also low adsorption enthalpy.

High-resolution neutron powder diffraction

In order to understand the exceptional performance of C_2H_2 adsorption in ELM-12, we performed high-resolution neutron powder diffraction on C_2D_2-loaded ELM-12. The Rietveld structural refinements were successfully performed to give a detailed structure of the C_2D_2 adsorption (Fig. 2). As shown in Fig. 2a, two preferential C_2H_2 adsorption sites were identified from the data. On site I, two C_2D_2 molecules are restricted in the pore centre, and each C_2D_2 is bound by two $CF_3SO_3^-$ anions from different nets through cooperative C–D···O H-bonding (2.43 and 2.44 Å; Fig. 2b), which enables the high C_2H_2 adsorption observed in ELM-12 at low pressure. On site II, the C_2D_2 molecule shows slightly weaker binding affinity as implied by its lower occupancy, with a C–D···F H-bonding from 2.29 Å to 3.31 Å (Fig. 2d). On both sites, the appropriate pore space provides a geometric optimal cage to restrict the linear C_2D_2 (3.3 × 3.3 × 5.7 $Å^3$) molecule. Thus, we can conclude that the exceptional performance of C_2H_2 adsorption in ELM-12 is attributed to its optimal pore sizes and polar functional moieties for binding C_2H_2. Structure comparison between bare ELM-12 and the C_2D_2-loaded structure reveals that the dynamic OTf^- accordingly adjusts its position/orientation upon C_2H_2 loading (Fig. S1†), while the overall crystal lattice stays nearly unchanged (the average interlayer distance increasing by only ~1.7%). Also, the geometric pore volume (0.141 cm^3 g^{-1}) remains almost the same as that of guest-free ELM-12 (0.138 cm^3 g^{-1}). The crystallographic data of C_2D_2-loaded ELM-12 is shown in Table S2.†

Dynamic separation of C_2H_2/C_2H_4 mixtures in ELM-12

Furthermore, we performed an actual breakthrough experiment to establish the feasibility of C_2H_2/C_2H_4 separations, in which

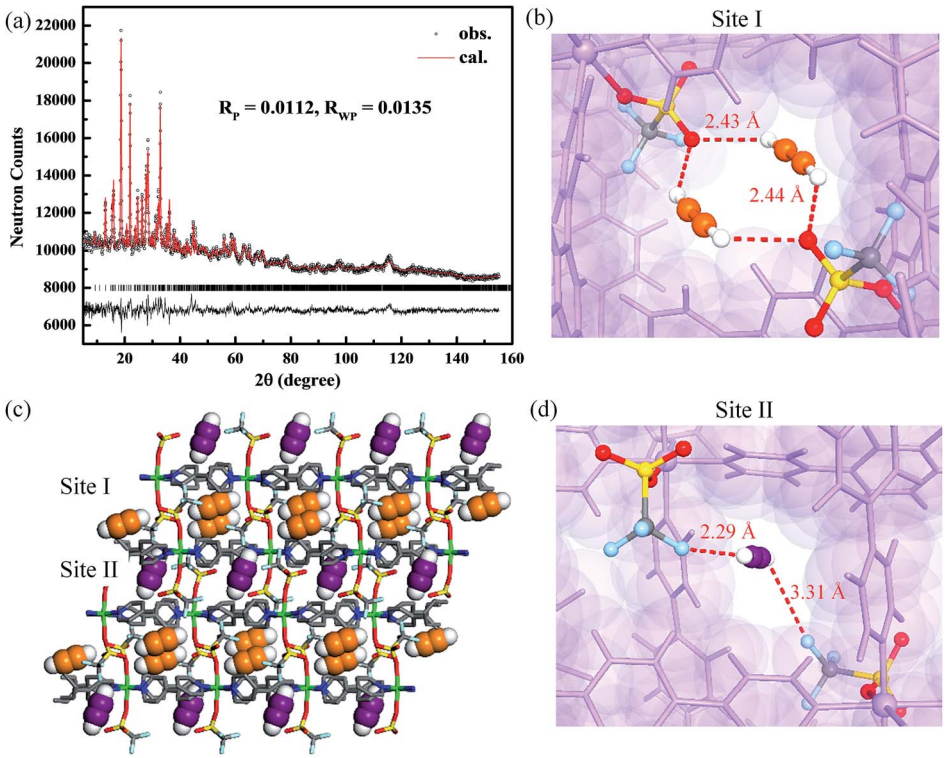

Fig. 2 (a) and (c) Rietveld refinement of the neutron powder diffraction ELM-12 ⊃ 2.5C_2D_2 at 298 K (Cu, green; C, gray; O, red; S, yellow; F, light blue). (b) and (d) The two preferential binding sites for C_2D_2 adsorption (sites I and II) in ELM-12.

C_2H_2/C_2H_4 (1/99 and 50/50) mixtures were used as feeds to mimic the industrial process conditions (Fig. 3 and S4†). As shown in Fig. 3, C_2H_4 firstly eluted through the bed to yield a polymer-grade gas, then, after a long period of time, C_2H_2 broke through from the adsorption bed. The capacity of C_2H_2 captured from the 1/99 mixture in ELM-12 was as high as 175 mmol per liter, and the concentration of C_2H_4 obtained from the outlet reached higher than 99.999%. Clearly, the C_2H_2 was efficiently removed by the ELM-12 material, reducing impurity concentration to lower than 10 ppm. In addition, ELM-12 exhibits excellent separation performance on the C_2H_2/C_2H_4 (50/50) mixture (Fig. S4†), and the concentration of C_2H_4 can be upgraded to higher than 99.995%.

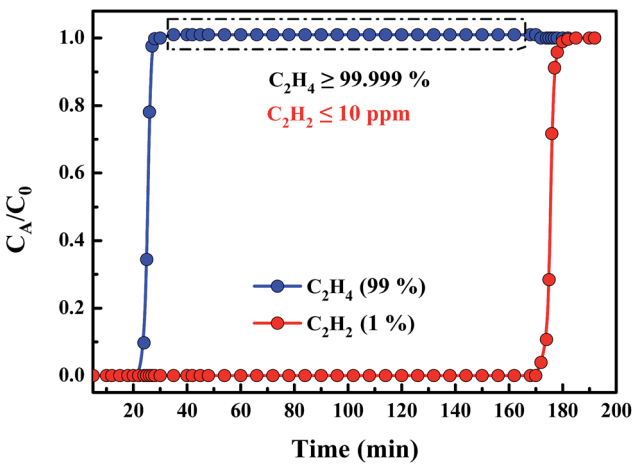

Fig. 3 Experimental column breakthrough curves of ELM-12 material for C_2H_2/C_2H_4 (1/99 mixture) separation at 298 K and 1 bar.

In normal industrial environments, an adsorbent should also possess good structural stability and regenerability. To ensure the cycling performance and regenerability of the ELM-12, we performed C_2H_2 and C_2H_4 adsorption and C_2H_2/C_2H_4 (1/99) cycling experiments at 1 bar and 298 K. As shown in the ESI (Fig. S5 and 6†), all C_2H_2 and C_2H_4 adsorption processes are completely reversible, and the adsorption cycling experiments further indicate no performance loss in C_2H_2 and C_2H_4 adsorption cycles. The cycling column breakthrough curves also show that ELM-12 can keep its separation ability for C_2H_2/C_2H_4 (1/99) separation mixtures over 20 cycles. Because of the low C_2H_2 adsorption heat, ELM-12 can be easily regenerated after the breakthrough experiments, and the adsorbed C_2H_2 can be fully removed under He flow for 30 minutes at 373 K. Furthermore, an aged sample was evaluated through PXRD and C_2H_2/C_2H_4 (1/99) separation at 298 K (Fig. S7†). The results showed that ELM-12 material possesses excellent structure stability, and its crystal structure and adsorption ability remain unchanged after two years of storage in regular sample vials.

Conclusions

We have identified a flexible-robust porous MOF (ELM-12) for the highly efficient removal of C_2H_2 from C_2H_4 mixtures. By using high-resolution neutron powder diffraction with Rietveld

structural refinements, we revealed the two primary C_2H_2 binding sites in ELM-12. The separation potential of ELM-12 has been established by IAST calculations and transient breakthrough experiments. Based on a fixed-bed adsorber, C_2H_4 mixtures can be purified to higher than 99.999%. The high efficiency of ELM-12 in removing trace C_2H_2 from important raw C_2H_2/C_2H_4 mixtures under ambient conditions to produce high-purity C_2H_4 indicates that this MOF might be potentially useful for this industrially important separation. It is expected that extensive research on porous MOFs will eventually lead to some practically useful materials at a reasonable cost in the near future for important hydrocarbon separation and purification processes.

Acknowledgements

We gratefully acknowledge the financial support from the National Natural Science Foundation of China (No. 21606163), Natural Science Foundation of Shanxi (No. 201601D021042), and Welch Foundation (grant AX-1730).

Notes and references

1 D. S. Sholl and R. P. Lively, *Nature*, 2016, **532**, 435–437.
2 X. Cui, K. Chen, H. Xing, Q. Yang, R. Krishna, Z. Bao, H. Wu, W. Zhou, X. Dong, Y. Han, B. Li, Q. Ren, M. J. Zaworotko and B. Chen, *Science*, 2016, **353**, 141–144.
3 T.-L. Hu, H. Wang, B. Li, R. Krishna, H. Wu, W. Zhou, Y. Zhao, Y. Han, X. Wang, W. Zhu, Z. Yao, S. Xiang and B. Chen, *Nat. Commun.*, 2015, **6**, 7328.
4 H. Furukawa, K. E. Cordova, M. O'Keeffe and O. M. Yaghi, *Science*, 2013, **341**, 1230444.
5 B. Chen, S. Xiang and G. Qian, *Acc. Chem. Res.*, 2010, **43**, 1115.
6 Y. Cui, B. Li, H. He, W. Zhou, B. Chen and G. Qian, *Acc. Chem. Res.*, 2016, **49**, 483–493.
7 B. Li, M. Chrzanowski, Y. Zhang and S. Ma, *Coord. Chem. Rev.*, 2016, **307**, 106–129.
8 Q.-L. Zhu and Q. Xu, *Chem. Soc. Rev.*, 2014, **43**, 5468–5512.
9 H. Wang, K. Yao, Z. Zhang, J. Jagiello, Q. Gong, Y. Han and J. Li, *Chem. Sci.*, 2014, **5**, 620–624.
10 J.-R. Li, R. J. Kuppler and H.-C. Zhou, *Chem. Soc. Rev.*, 2009, **38**, 1477–1504.
11 Q.-G. Zhai, X. Bu, C. Mao, X. Zhao, L. Daemen, Y. Cheng, A. J. Ramirez-Cuesta and P. Feng, *Nat. Commun.*, 2016, **7**, 13645.
12 C. Wang, D. Liu and W. Lin, *J. Am. Chem. Soc.*, 2013, **135**, 13222–13234.
13 S.-C. Xiang, Z. Zhang, C.-G. Zhao, K. Hong, X. Zhao, D.-R. Ding, M.-H. Xie, C.-D. Wu, M. C. Das, R. Gill, K. M. Thomas and B. Chen, *Nat. Commun.*, 2011, **2**, 204.
14 A. Cadiau, K. Adil, P. M. Bhatt, Y. Belmabkhout and M. Eddaoudi, *Science*, 2016, **353**, 137–140.
15 S. Nandi, S. Collins, D. Chakraborty, D. Banerjee, P. K. Thallapally, T. K. Woo and R. Vaidhyanathan, *J. Am. Chem. Soc.*, 2017, **139**, 1734–1737.
16 F. Luo, C. Yan, L. Dang, R. Krishna, W. Zhou, H. Wu, X. Dong, Y. Han, T.-L. Hu, M. O'Keeffe, L. Wang, M. Luo, R.-B. Lin and B. Chen, *J. Am. Chem. Soc.*, 2016, **138**, 5678–5684.
17 Z. Bao, G. Chang, H. Xing, R. Krishna, Q. Ren and B. Chen, *Energy Environ. Sci.*, 2016, **9**, 3612–3641.
18 S. Yang, A. J. Ramirez-Cuesta, R. Newby, V. Garcia-Sakai, P. Manuel, S. K. Callear, S. I. Campbell, C. C. Tang and M. Schröder, *Nat. Chem.*, 2015, **7**, 121–129.
19 A. J. Howarth, M. J. Katz, T. C. Wang, A. E. Platero-Prats, K. W. Chapman, J. T. Hupp and O. K. Farha, *J. Am. Chem. Soc.*, 2015, **137**, 7488–7494.
20 A. Cadiau, K. Adil, P. M. Bhatt, Y. Belmabkhout and M. Eddaoudi, *Science*, 2016, **353**, 137–140.
21 P. Nugent, Y. Belmabkhout, S. D. Burd, A. J. Cairns, R. Luebke, K. Forrest, T. Pham, S. Ma, B. Space, L. Wojtas, M. Eddaoudi and M. J. Zaworotko, *Nature*, 2013, **495**, 80–84.
22 E. D. Bloch, W. L. Queen, R. Krishna, J. M. Zadrozny, C. M. Brown and J. R. Long, *Science*, 2012, **335**, 1606–1610.
23 P.-Q. Liao, W.-X. Zhang, J.-P. Zhang and X.-M. Chen, *Nat. Commun.*, 2015, **6**, 8697.
24 A. Kondo, H. Kajiro, H. Noguchi, L. Carlucci, D. M. Proserpio, G. Ciani, K. Kato, M. Takata, H. Seki, M. Sakamoto, Y. Hattori, F. Okino, K. Maeda, T. Ohba, K. Kaneko and H. Kanoh, *J. Am. Chem. Soc.*, 2011, **133**, 10512–10522.
25 A. Kondo, H. Noguchi, L. Carlucci, D. M. Proserpio, G. Ciani, H. Kajiro, T. Ohba, H. Kanoh and K. Kaneko, *J. Am. Chem. Soc.*, 2007, **129**, 12362–12363.
26 L. Li, R.-B. Lin, R. Krishna, X. Wang, B. Li, H. Wu, J. Li, W. Zhou and B. Chen, *J. Am. Chem. Soc.*, 2017, **139**, 7733–7736.
27 L. Li, R. Krishna, Y. Wang, J. Yang, X. Wang and J. Li, *J. Mater. Chem. A*, 2016, **4**, 751–755.
28 M. L. Foo, R. Matsuda, Y. Hijikata, R. Krishna, H. Sato, S. Horike, A. Hori, J. Duan, Y. Sato, Y. Kubota, M. Takata and S. Kitagawa, *J. Am. Chem. Soc.*, 2016, **138**, 3022–3030.
29 S. Horike, Y. Inubushi, T. Hori, T. Fukushima and S. Kitagawa, *Chem. Sci.*, 2012, **3**, 116–120.
30 L. Hamon, P. L. Llewellyn, T. Devic, A. Ghoufi, G. Clet, V. Guillerm, G. D. Pirngruber, G. Maurin, C. Serre, G. Driver, W. V. Beek, E. Jolimaître, A. Vimont, M. Daturi and G. Férey, *J. Am. Chem. Soc.*, 2009, **131**, 17490–17499.
31 F.-X. Coudert, C. Mellot-Draznieks, A. H. Fuchs and A. Boutin, *J. Am. Chem. Soc.*, 2009, **131**, 11329–11331.
32 C. Gücüyener, J. van den Bergh, J. Gascon and F. Kapteijn, *J. Am. Chem. Soc.*, 2010, **132**, 17704–17706.
33 L. Li, Y. Wang, J. Yang, X. Wang and J. Li, *J. Mater. Chem. A*, 2015, **3**, 22574–22583.
34 R.-B. Lin, L. Li, H. Wu, H. Arman, B. Li, R.-G. Lin, W. Zhou and B. Chen, *J. Am. Chem. Soc.*, 2017, **139**, 8022–8028.

Supporting Information

Efficient separation of ethylene from acetylene/ethylene mixtures by a flexible-robust metal-organic framework

Libo Li,[a,b,e] Rui-Biao Lin,[b] Rajamani Krishna,[c] Xiaoqing Wang,[a,e] Bin Li,[b] Hui Wu,[d] Jinping Li,[a,e,*] Wei Zhou,[d,*] and Banglin Chen[b,*]

[a]College of Chemistry and Chemical Engineering, Taiyuan University of Technology, Taiyuan 030024, Shanxi, P. R. China

[b]Department of Chemistry, University of Texas at San Antonio, One UTSA Circle, San Antonio, TX 78249-0698, United States

[c]Van 't Hoff Institute for Molecular Sciences, University of Amsterdam, Science Park 904, 1098 XH Amsterdam, The Netherlands

[d]NIST Center for Neutron Research, National Institute of Standards and Technology, Gaithersburg, MD 20899-6102, United States

[e]Shanxi Key Laboratory of Gas Energy Efficient and Clean Utilization, Taiyuan 030024, Shanxi, P. R. China

Table of Contents

1. Experimental section

1.1 Synthesis and characterization of ELM-12

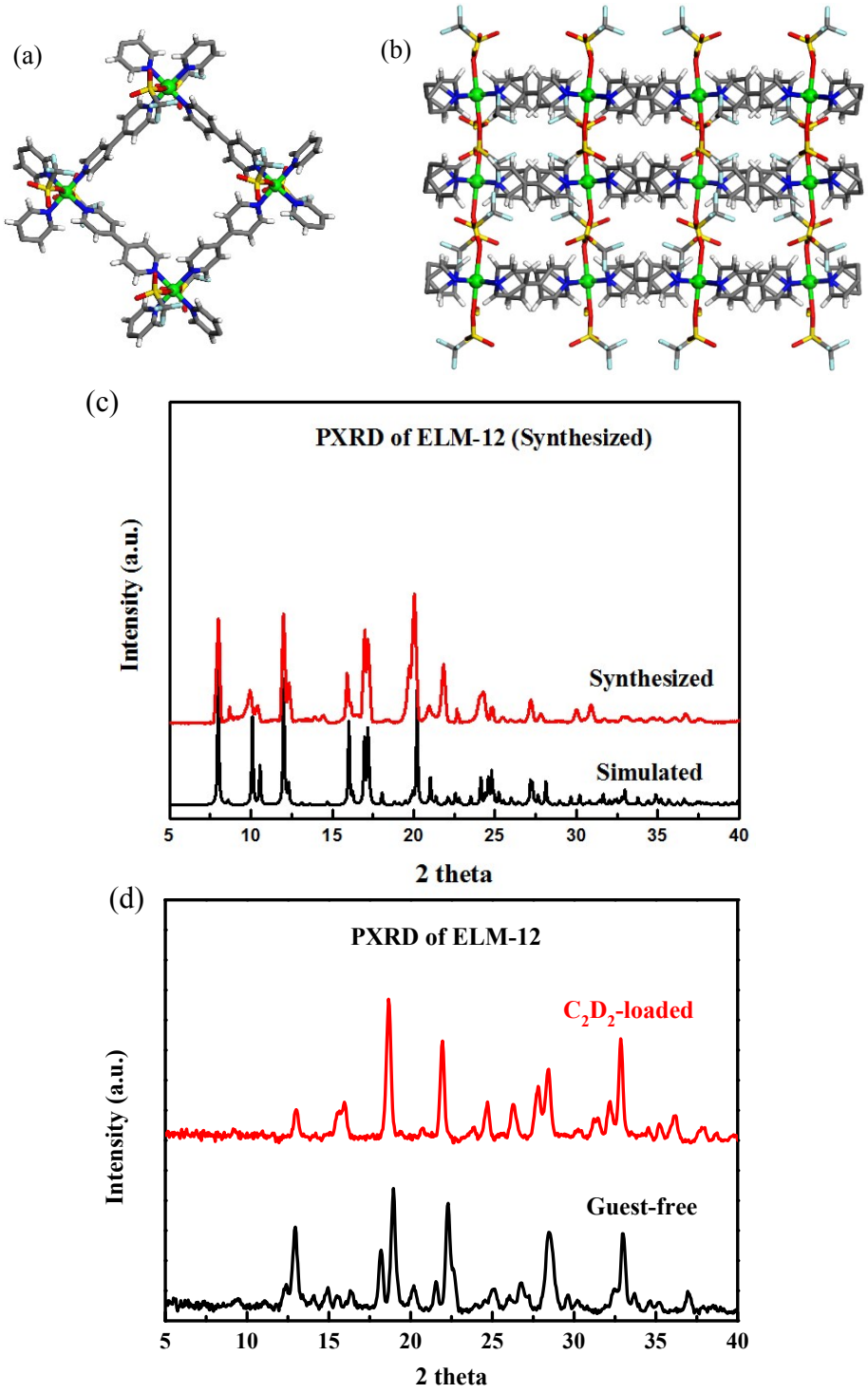

Fig S1. (a, b) Schematic diagram of the structure of ELM-12. (c) Powder X-ray diffraction (PXRD) patterns of synthesized ELM-12 sample. (d) PXRD patterns of guest-free and C_2D_2-loaded ELM-12 samples. (Cu, green; C, gray; O, red; H, white; S, yellow; F, blue).

1.2 Breakthrough experiments

The breakthrough curves were measured on a homemade apparatus for gases mixtures C_2H_2/C_2H_4 (1/99 and 50/50) at 298 K and 1 bar. The gas flows were controlled at the inlet by a mass flow meter as 2 mL/min, and a gas chromatograph (TCD-Thermal Conductivity Detector) continuously monitored the effluent gas from the adsorption bed. Prior to every breakthrough experiment, we activated the sample by flushing the adsorption bed with helium gas for 2 hours at 373 K. Subsequently, the column was allowed to equilibrate at the measurement rate before we switched the gas flow.

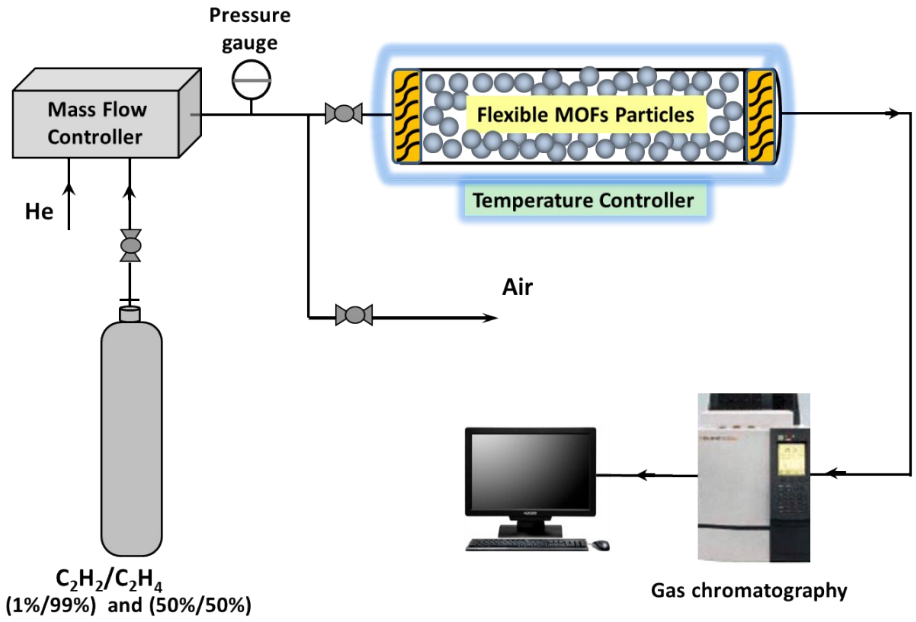

Fig. S2 Breakthrough experiment apparatus.

2. Calculation of the separation potential of ELM-12

2.1 Fitting of pure component isotherms

The experimentally measured excess loadings for C_2H_2 and C_2H_4 at temperatures of 273 and 298 K for ELM-12 were fitted with the dual-Langmuir-Freundlich isotherm model

$$q = q_{A,sat}\frac{b_A p^{\nu_A}}{1+b_A p^{\nu_A}} + q_{B,sat}\frac{b_B p^{\nu_B}}{1+b_B p^{\nu_B}} \quad (1)$$

with T-dependent parameters b_A, and b_B

$$b_A = b_{A0}\exp\left(\frac{E_A}{RT}\right); \quad b_B = b_{B0}\exp\left(\frac{E_B}{RT}\right) \quad (2)$$

The parameters are provided in table S1.
For all other MOFs, the isotherm data are taken from Cui et al.[1]

	Site A				Site B			
	$q_{A,sat}$ mol kg^{-1}	b_{A0} Pa$^{-\nu_i}$	E_A kJ mol^{-1}	ν_A dimensionless	$q_{B,sat}$ mol kg^{-1}	b_{B0} Pa$^{-\nu_i}$	E_B kJ mol^{-1}	ν_B dimensionless
C_2H_2	0.65	8.7×10^{-6}	4.5	1.36	2.5	1.87×10^{-9}	24.6	1
C_2H_4	1.45	1.54×10^{-8}	18	1				

Table S1. Dual-Langmuir-Freundlich fitting parameters for C_2H_2 and C_2H_4 isotherms.

Reference

[1] X. Cui, K. Chen, H. Xing, Q. Yang, R. Krishna, Z. Bao, H. Wu, W. Zhou, X. Dong, Y. Han, B. Li, Q. Ren, M. J. Zaworotko, B. Chen, *Science*, **2016**, 353, 141-144.

2.2 IAST calculations of adsorption selectivities

We consider the separation of binary C_2H_2/C_2H_4 mixtures. The adsorption selectivity for C_2H_2/C_2H_4 separation is defined by

$$S_{ads} = \frac{q_1/q_2}{p_1/p_2} \tag{3}$$

q_1, and q_2 are the molar loadings in the adsorbed phase in equilibrium with the bulk gas phase with partial pressures p_1, and p_2.

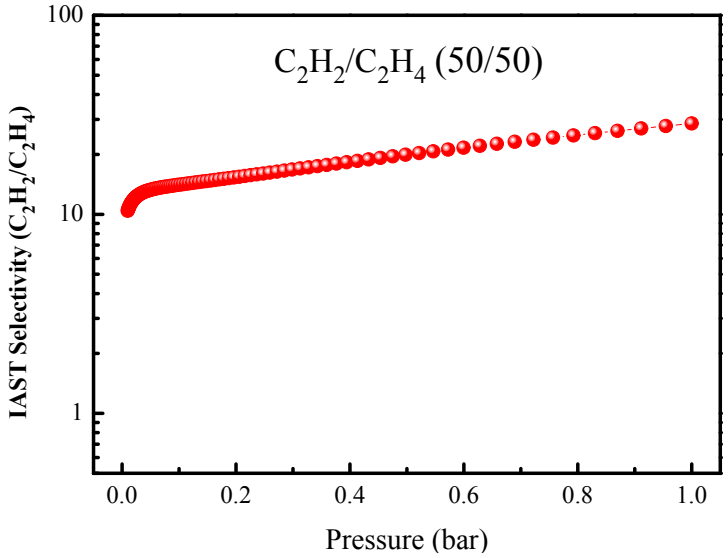

Fig. S3 IAST calculations of the adsorption selectivity of C_2H_2/C_2H_4 (50/50) mixtures on ELM-12.

Notation

b_A	Langmuir-Freundlich constant for species *i* at adsorption site A, $Pa^{-\nu_{iA}}$
b_B	Langmuir-Freundlich constant for species *i* at adsorption site B, $Pa^{-\nu_{iB}}$
c_i	molar concentration of species *i* in gas mixture, mol m^{-3}
c_{i0}	molar concentration of species *i* in gas mixture at inlet to adsorber, mol m^{-3}
E	energy parameter, J mol^{-1}
L	length of packed bed adsorber, m
p_i	partial pressure of species *i* in mixture, Pa
p_t	total system pressure, Pa
q_i	component molar loading of species *i*, mol kg^{-1}
Q_{st}	isosteric heat of adsorption, J mol^{-1}
t	time, s
T	absolute temperature, K
u	superficial gas velocity in packed bed, m s^{-1}

Greek letters

ε	voidage of packed bed, dimensionless
ν	Freundlich exponent, dimensionless
ρ	framework density, kg m^{-3}
τ	time, dimensionless

3. Breakthrough curves for C_2H_2/C_2H_4 separation

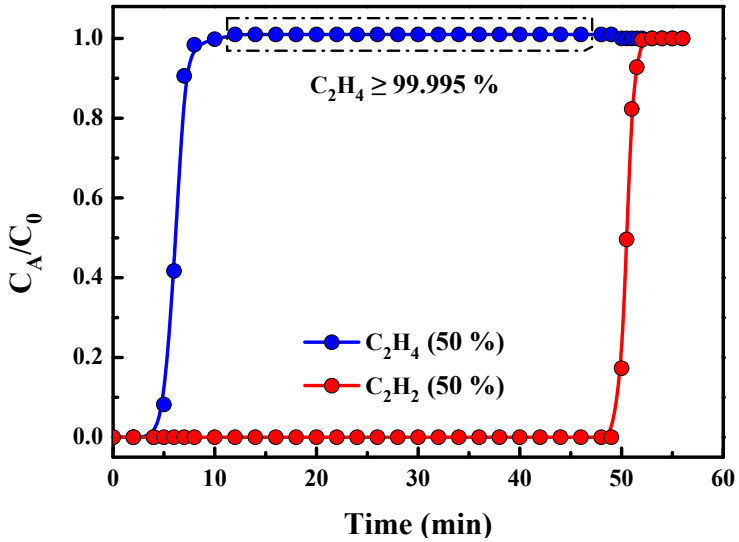

Fig. S4 Experimental breakthrough curves of C_2H_2/C_2H_4 (50/50) mixtures separation for ELM-12 materials at 298 K and 1 bar.

4. Adsorption cycling experiments for ELM-12

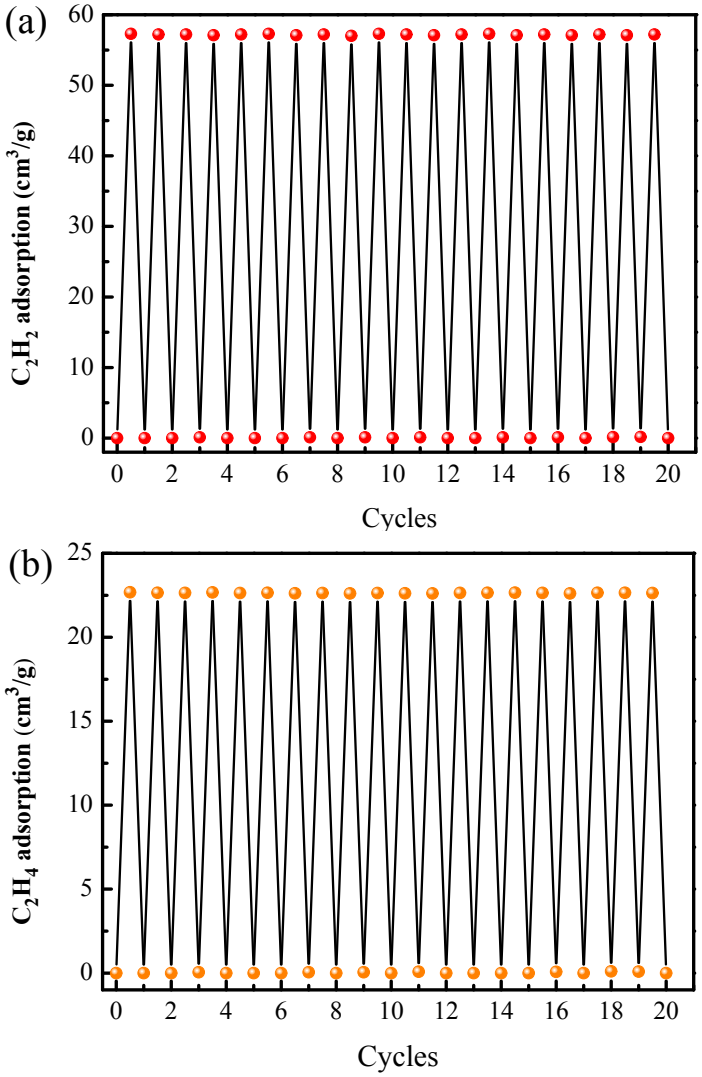

Fig. S5 C_2H_2 (a) and C_2H_4 (b) adsorption cycles for ELM-12. After each adsorption process, sample was evacuated under 10^{-6} bar for 30 minutes.

5. Separation cycling experiments for ELM-12

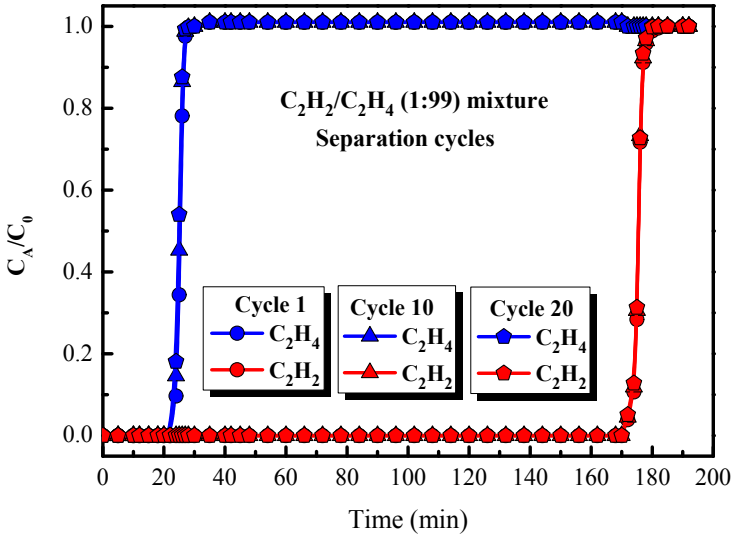

Fig. S6 (a) Cycling column breakthrough curves of C_2H_2/C_2H_4 separation (1/99) for ELM-12 at 298 K and 1 bar. The breakthrough experiments were carried out at a flow rate of 2 mL/min. Regeneration with He flow (100 mL/min) for 30 minutes at 373 K.

6. Structural stability experiments for ELM-12

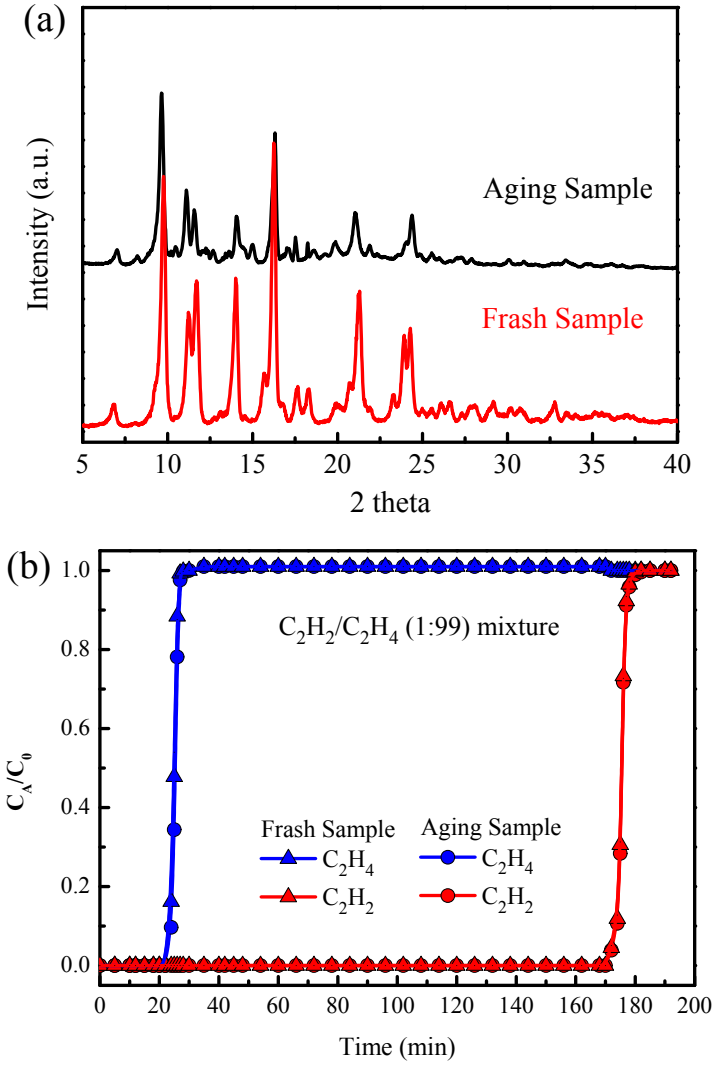

Fig. S7 (a) PXRD and (b) breakthrough experiment of C_2H_2/C_2H_4 (1/99) mixture for ELM-12 samples (fresh sample and two-years aging sample), respectively.

Crystal data	ELM-12 (Guest-free)[#]	ELM-12 (C_2D_2)
system	monoclinic	monoclinic
space group	C2/c	C2/c
MF	$C_{22}H_{16}CuF_6N_4O_6S_2$	$C_{24.43}H_{16}CuD_{2.43}F_6N_4O_6S_2$
FW	674.05	708.19
a/Å	27.080	27.315
b/Å	15.096	14.930
c/Å	16.136	16.516
α/^{o}	90.00	90.00
β/^{o}	111.344	110.786
γ/^{o}	90.00	90.00
volume/Å^3	6144	6296.8
Z	8	8
density/g/cm^3	1.457	1.422
theoretical pore volume/cm^3/g	0.138[a]	0.141[a]
refinement parameters	R_1 = 0. 1415, wR_2 = 0.3556	R_p = 0.0112, R_{wp} = 0.0135

a Calculated on the basis of the MOF crystal structures using PLATON software.

Table S2. Comparison of the Crystallographic and Refinement Parameters for Guest-free ELM-12[#] and C_2D_2-loaded ELM-12.

[#] Kondo, A. et al. *J. Am. Chem. Soc.*, **2007**, 129, 12362.

†